



# Removal of malachite green from aqueous solution by magnetic $\text{CuFe}_2\text{O}_4$ nano-adsorbent synthesized by one pot solution combustion method

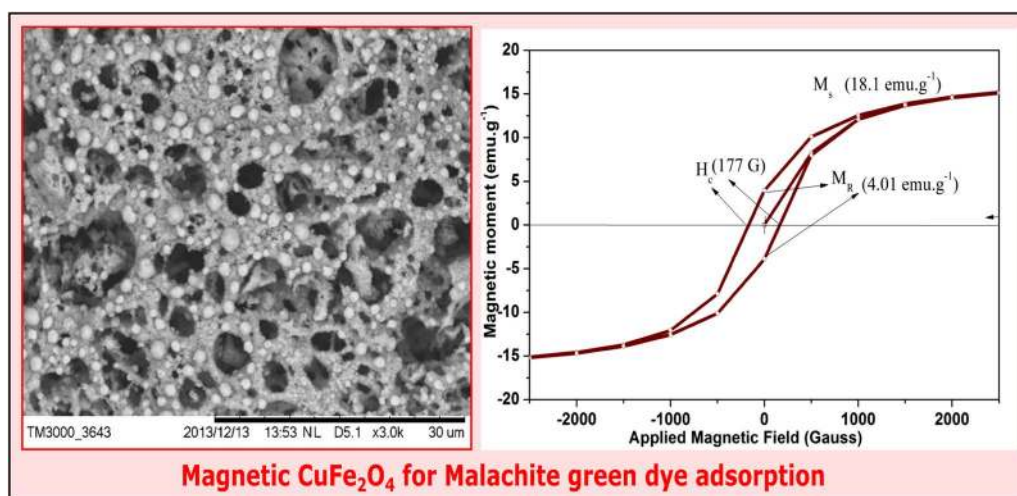
Bincy Rose Vergis<sup>1,2</sup> · R. Hari Krishna<sup>1</sup> · Nagaraju Kottam<sup>1</sup> · B. M. Nagabhushana<sup>1</sup> · R. Sharath<sup>3</sup> · B. Darukaprasad<sup>4</sup>

Received: 19 July 2017 / Accepted: 1 December 2017 / Published online: 15 December 2017  
© The Author(s) 2017. This article is an open access publication

## Abstract

In the present investigation nano copper ferrite,  $\text{CuFe}_2\text{O}_4$  (CF) is synthesized by one pot energy saving solution combustion synthesis. The combustion derived copper ferrite nanoadsorbent is characterized by powder X-ray diffraction, Fourier transform infra-red spectroscopy, scanning electron microscopy, transmission electron microscopy and UV–Vis spectroscopy. The magnetic behavior is studied by Vibrating sample magnetometer measurements and the results shows it's a soft ferromagnet with low saturation magnetization and coercive effect. CF nanopowder is used as good magnetically separable nanoadsorbent. Adsorption property is evaluated by the removal of malachite green, a dye which is widely used by many industries, from its aqueous solution. Various parameters like contact time (5–30 min), adsorbent loading (0–45 mg) are investigated systematically by batch experiments. Adsorption isotherms and kinetic studies also conducted which shows that the adsorption follows pseudo second order mechanism. The experimental data fitted well with the Langmuir isotherm ( $R^2 = 0.978$ ), yielding a maximum adsorption capacity of 22 mg/g. The optimum adsorbent dose was found to be 40 mg/L and stirring time experiment reveals that 85% of decolourization was observed for 30 min of stirring at neutral pH which is much more efficient than those reported in literature.

## Graphical abstract



**Keywords**  $\text{CuFe}_2\text{O}_4$  · Solution combustion · VSM studies · Adsorption · Kinetics

Extended author information available on the last page of the article

## Introduction

Various Industries like pharmaceutical, food, printing and textile industries use various dyes as redox indicators, biological stains [1–4]. These industries across the world prefer dumping millions of tons of dye effluents into rivers, as dumping is cheaper than recycling. Many dyes like azo dyes, fluorescein dyes are highly toxic and poisonous. For example azo dyes which are widely used as an industrial colorants in textiles cause toxic effects in human liver cells and also carcinogenic. Fluorescein dyes have been reported to be highly cytotoxic for mammalian tissues, which trigger morphological and genetic alterations [5]. Therefore the disposal of organic dyes into water bodies is a matter of concern. Malachite green is extensively used in many industries as a dye for leather, textiles and also in aquaculture industry to control fish parasites and disease. The use has increased so much because of its easy preparation and low manufacturing cost. Malachite green is classified as a class II health hazard and they pose toxicity (mutagenicity, genotoxicity) to the aquatic organisms like fish, algae, bacteria etc. and it's proved to be highly carcinogenic and is banned by many countries [6].

The removal of organic pollutants and dyes from industries remain as a challenge as these dye molecules are difficult to decompose. Varieties of organic and heavy metal pollutants were removed by nano adsorbents by various research groups [7–10]. Various methods have been devised for the degradation of dyes in aqueous solution. These include adsorption, biological treatment, advanced oxidation process (AOPS), electrochemical deposition and photocatalysis [11–15]. All the above said methods are successful to certain extent.

Spinel is the class of compounds of the type  $M^{2+}M_2^{3+}O_4$ , which has attracted researches because of its versatile properties and applications in various fields [16]. When  $M^{3+} = Fe$ , we get spinel ferrites with the general formula  $MFe_2O_4$  and the transition metal spinel ferrites are obtained when  $M = Cu, Fe, Mn, Ni, Zn$  etc. These spinel ferrites are studied more due to their magnetic property and semiconducting property [17]. Among all the ferrites, spinel copper ferrite is one of the most important ferrite and finds application as ferro fluids, humidity sensor, gas sensor [18] as catalyst for organic reactions and are used in multilayer chip induction, high speed digital tape or recording disks, rod antennas etc. [19]. In this study, we make use of magnetic property of nano crystalline copper ferrite in the removal of dyes from effluents by adsorption as this property of ferrites is not much investigated. Adsorption property of ferrites depends on its structure and composition which in turn depends on the method of synthesis and the distribution of cations in the crystal

lattice [20]. The diverse routes available or adopted to prepare nano-sized spinel ferrites are ball-milling, sol-gel, co-precipitation, hydrothermal etc. [21]. However, these methods are tedious and require lot of time and are expensive.

Here we adopted solution combustion synthesis (SCS) route, which is an excellent technique for preparing nanocrystalline metal oxides with high surface area. This technique is advantageous due to its low processing temperature, short reaction time, and good yield and also we get the particles in its nanocrystalline size [22]. SCS is based on the exothermic reaction and once the reaction is initiated, it undergoes self-sustaining combustion. Thus this method is adapted to synthesis spinel copper ferrite in its nanosize with highly porous structure which is required for good adsorption property [23]. In our study we adopted adsorption method to remove dye from the effluent as its easy and less expensive technique since no energy sources is involved in the process. In most of these cases nanoparticles are used as the adsorbent or as the catalyst for the removal of dye, but these nanoparticles find difficulty in the removal from the treated water, because of its very small size. To overcome this problem the use of magnetic nanomaterials as adsorbent was proposed, wherein these nanoparticles can be removed from the treated water by using an external magnet. Several works has been reported in this direction [24]. Numerous ecofriendly applications in catalysis have been addressed through magnetically recoverable and recyclable nanocatalysts for reduction, oxidation and condensation reactions [25]. This prompted us to investigate the use of magnetically separable spinel copper ferrite nanoparticle as an adsorbent for dye molecule.

## Materials and methods

Copper nitrate  $Cu(NO_3)_2 \cdot 3H_2O$ , ferric nitrate  $Fe(NO_3)_3 \cdot 9H_2O$ , glycine ( $CH_2NH_2COOH$ ) and malachite green are purchased from SD fine chemicals and all the chemicals are of analytical grade with 99% purity and are used without further purification. Double distilled water was used for the entire experimental procedure.

## Synthesis of copper ferrite

Spinel copper ferrite is prepared by one pot solution combustion method using glycine as fuel. This is a wet chemical process, wherein the fuel, an organic compound and an oxidizer, the metal nitrates of the oxide to be prepared are used as precursors. The typical combustion synthesis procedure followed for the preparation of spinel copper ferrite (CF) is as follows.

$\text{Cu}(\text{NO}_3)_2 \cdot 3\text{H}_2\text{O}$  and  $\text{Fe}(\text{NO}_3)_3 \cdot 9\text{H}_2\text{O}$  in the ratio 1:2 is mixed with stoichiometric quantity of glycine calculated by propellant chemistry calculations and is taken in a cylindrical petri dish of 300 mL capacity. To this mixture of nitrates and fuel, ~ 20 mL of doubled distilled water was added and stirred using a magnetic stirrer to get a homogeneous solution. The resulting clear solution was introduced into a pre-heated muffle furnace maintained at  $500 \pm 10$  °C. First solution boils followed by dehydration with the evolution of large amount of gases. At the end of dehydration highly viscous gel was obtained which catches fire at one place and spreads all over the reaction mixture with flames. This combustion sustains for ~ 1–2 min and results in the formation of highly voluminous porous product.

### Point of zero charge

The  $\text{pH}_{\text{PZC}}$  (point of zero charge) is the pH when the charge on the surface of  $\text{CuFe}_2\text{O}_4$  is zero. The procedure of  $\text{pH}_{\text{PZC}}$  drift method [26] could be described as follows: to a series of 250 mL conical flasks, 50 mL of 0.01 N NaCl was added. Then, the initial solution pH values (say pH initial) were adjusted in range between 2 and 9 with intervals of one using 0.01 N HCl solutions and 0.01 N NaOH. After constant value of  $\text{pH}_{\text{initial}}$  had been reached, 0.010 g of  $\text{CuFe}_2\text{O}_4$  was added into each conical flask and capped them immediately. These solutions were stirred for 12 h to reach equilibrium. After 12 h, pH of solution was measured noted as  $\text{pH}_{\text{final}}$ . The  $\text{pH}_{\text{PZC}}$  of  $\text{CuFe}_2\text{O}_4$  is the point when  $\text{pH}_{\text{initial}} = \text{pH}_{\text{final}}$ .

### Characterization

Copper ferrite was characterized by powder X-ray diffraction technique (PXRD) PANalytical with diffractometer system, XPERT-3 operated at 40 kV and 30 mA. Surface morphology was characterized by a field emission scanning electron microscope (FESEM, Hitachi S4800) and a high resolution transmission electron microscope (HR-TEM, FEI Tecnai G2 F20). Further the structure was analyzed by Fourier transform infrared (FTIR). The magnetic measurements were carried out at room temperature using vibrating sample magnetometer, VSM 7410 (Lake Shore Cryotronics, Inc.).

## Results and discussion

### Characterization of copper ferrite

#### Powder X-ray diffraction technique (PXRD)

The phase composition of the sample synthesized was determined by powder X-ray diffraction. XRD graph given in Fig. 1 is analyzed for its phase purity and crystallographic

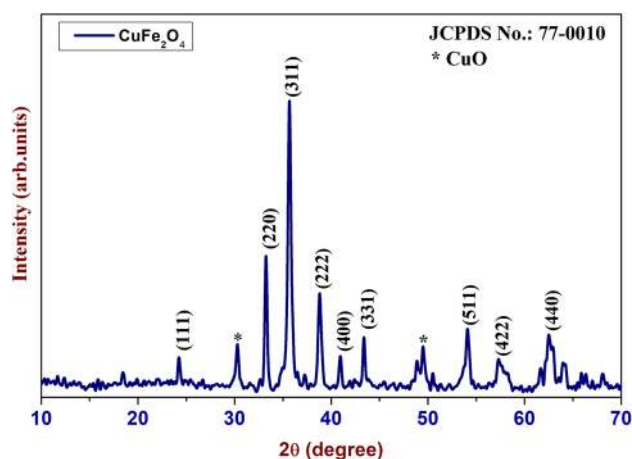


Fig. 1 XRD pattern of solution combustion derived copper ferrite

identity of the copper ferrite. The graph shows all the peaks of  $\text{CuFe}_2\text{O}_4$  and matches with that of standard JCPDS file No: 00-077-0010 [27]. The diffraction peaks with the miller indices in the XRD pattern suggests that the prepared  $\text{CuFe}_2\text{O}_4$  has a cubic spinel structure, in which  $\text{Cu}^{2+}$  ions occupy the tetrahedral sites and  $\text{Fe}^{3+}$  ions occupy the octahedral sites of the crystal lattice. Along with this there is a traces of  $\text{CuO}$  corresponds to the JCPDS card No. 48-1548 as an additional phase. The  $d$ -spacing ( $d_{hkl}$ ) and lattice constant ( $a$ ) have been calculated using most intense reflection (311) from equation,  $a = d_{hkl}(h^2 + k^2 + l^2)^{0.5}$  where  $h, k, l$  are the miller indices corresponding to respective planes [28]. The estimated ‘ $a$ ’ and  $d_{hkl}$  values were found to be 8.4 nm and 2.5 Å respectively which are in good agreement with the standard values as reported elsewhere [29]. The crystallites size ( $D$ ) has been calculated using line broadening of most intense (311) peak using Scherrer’s equation [30] as given in Eq. (1)

$$D = \frac{0.89 \times \lambda}{\beta \cos \theta} \quad (1)$$

Where  $D$  is the crystallite size,  $\beta$  is the full width half maximum,  $\lambda$  is the X-ray wavelength and  $\theta$  is the Bragg’s angle. The average crystallite size estimated was ~ 17 nm.

#### Fourier transform infrared spectrum (FTIR)

The FTIR spectra recorded for  $\text{CuFe}_2\text{O}_4$  nanoparticles in the range between 4000 and 450  $\text{cm}^{-1}$  are shown in Fig. 2. The spectra give information about the chemical, molecular structure and impurities present in the synthesized ferrites. Absorption bands appear one at 528  $\text{cm}^{-1}$ , which is attributed to stretching vibration of octahedral group Fe–O stretching [31] and another band at 451  $\text{cm}^{-1}$  are attributed to the tetrahedral group Cu–O stretching bands [32].



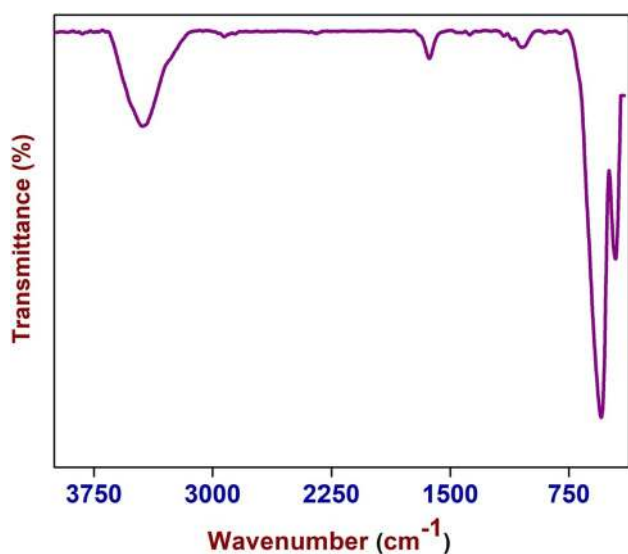


Fig. 2 FTIR spectrum of solution combustion derived copper ferrite

The other peaks at  $3425$  and  $1651\text{ cm}^{-1}$  corresponds to the adsorbed  $\text{H}_2\text{O}$ ,  $\text{NO}_3$  [33] onto the surface of the spinel ferrites respectively. The adsorption of  $\text{H}_2\text{O}$  is typical of nano-materials and the presence of  $\text{NO}_3$  might be due to the nature of precursors used.

### Specific surface area

Specific surface area (SSA) is one of the essential material parameters for nano adsorbents. Various parameters determine the surface area of the adsorbent such as shape, particle size, surface morphology and size distribution. In addition porosity is also one of the important factor on which SSA depends. It is well reported in the literature that solution combustion derived products exhibits high surface area due to the fact that the exothermicity during the combustion

is long enough for the particle formation but too short for grain growth [34]. Figure 3 shows the surface area and pore size distribution of the  $\text{CuFe}_2\text{O}_4$  adsorbent evaluated from nitrogen adsorption and desorption isotherms. The BET surface area of  $\text{CuFe}_2\text{O}_4$  derived from solution combustion synthesis is found to be  $128\text{ m}^2/\text{g}$ . Figure 3b shows the pore size distribution which are calculated using the Barrett–Joyner–Halenda (BJH) model. For this calculation,  $\text{N}_2$  isotherms are used. The pore size distribution of the sample show that pore diameter  $5\text{--}30\text{ \AA}$  with a maximum at about  $\sim 5\text{ \AA}$ .

### Scanning electron microscopy (SEM)

The morphology of the prepared sample was performed using SEM (scanning electron microscope). Figure 4a, b gives the images of copper ferrite at different magnifications. The secondary electron images were taken at different magnifications to study the morphological and their composition of elements was analyzed by EDAX (not shown here). It can be seen from SEM micrographs that the morphology of the samples shows agglomerated clusters with huge voids and pores. The agglomeration of the product is typical of the solution combustion product and is attributed to the higher temperature produced during synthesis. The voids and porous structure can be attributed to the gaseous by products during exothermic reaction [35].

### TEM studies

Figure 5a–c shows the TEM and HRTEM images of copper ferrite respectively. From the images it is clear that combustion derived copper ferrite show highly agglomerated mass of particles with narrow size distribution. It is important to mention here that due to high exothermic nature of combustion using glycine as fuel resulted in local sintering of

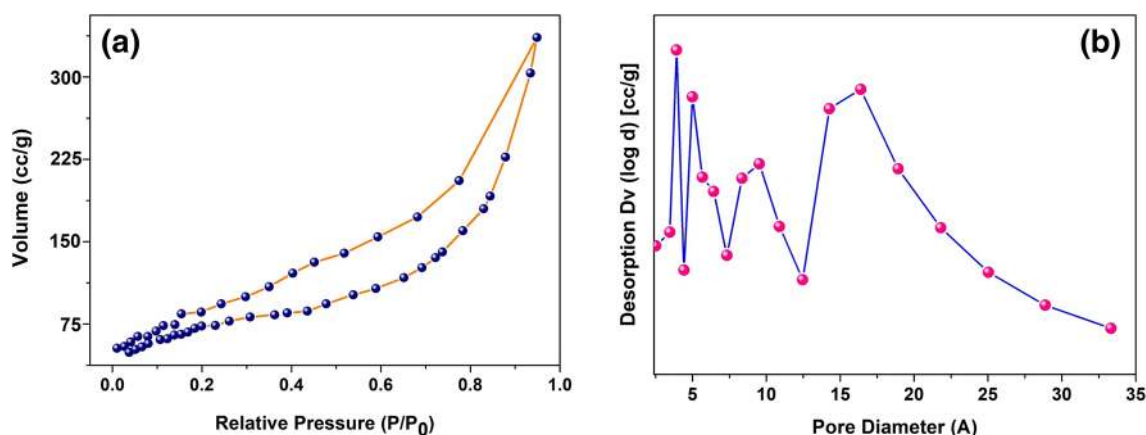
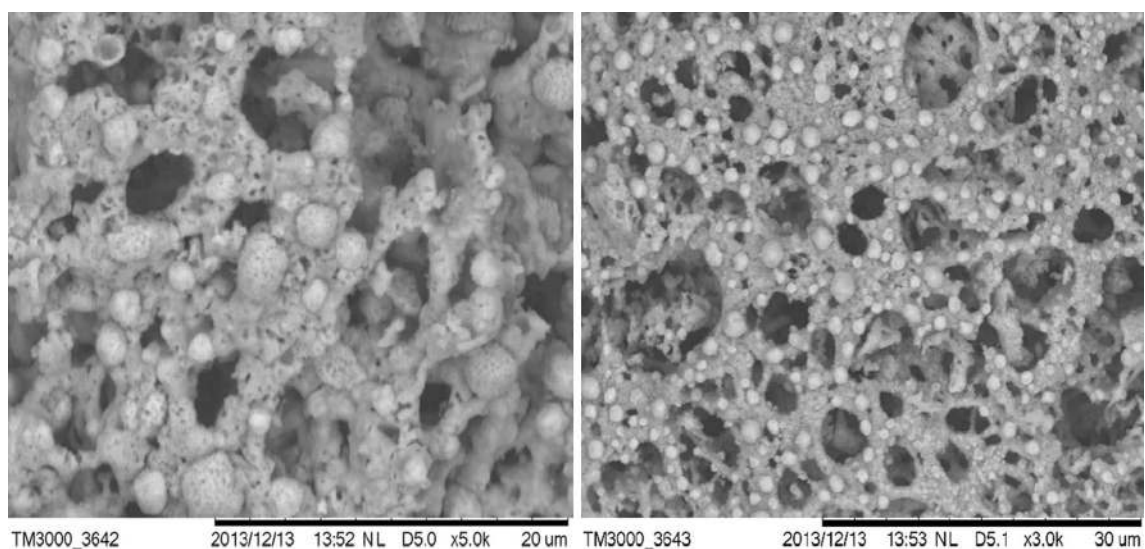


Fig. 3 a Nitrogen adsorption/desorption isotherms and b the pore size distribution of  $\text{CuFe}_2\text{O}_4$  particles obtained through the Barrett–Joyner–Halenda method







**Fig. 4** SEM images of copper ferrite low and high magnification respectively

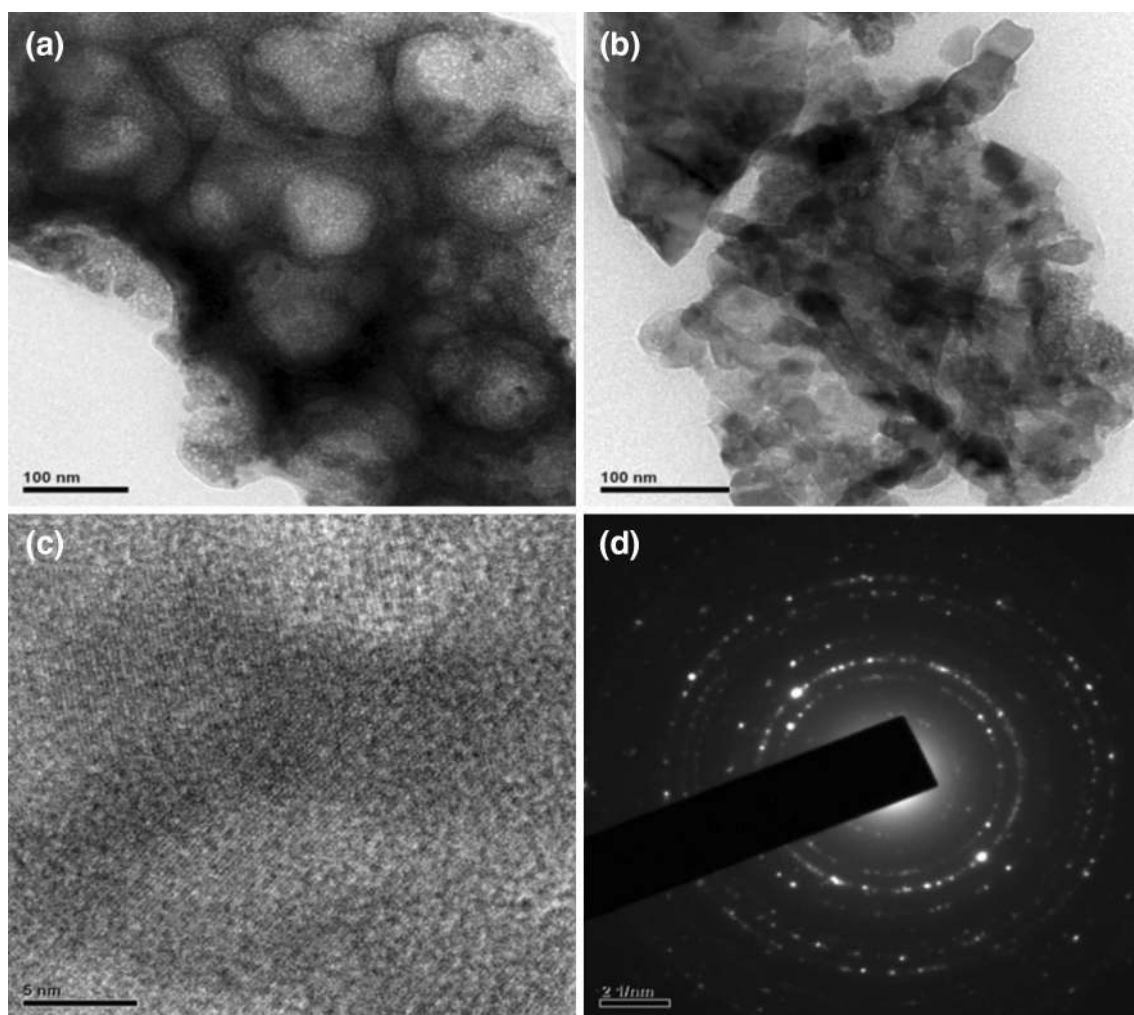


**Fig. 5** a, b TEM, c HRTEM and d SAED pattern of copper ferrite

particles. Hence, individual particles are not clearly visible in the presented TEM images. However, careful observation of TEM micrograph reveals that agglomerated particles of ~ 40–50 nm forms porous mass. The diffraction pattern (SAED) of the as-prepared copper ferrite indicates that  $\text{CuFe}_2\text{O}_4$  nanoparticles show polycrystalline nature clear circular spots. The crystallinity of the synthesized nanoparticles was also supported by the clear lattice fringes of ~ 0.25 nm in HRTEM image.

## Magnetic studies

Figure 6 represents room temperature M-H curves for  $\text{CuFe}_2\text{O}_4:\text{CuO}$  sample. The presence of excess  $\text{Cu}^{2+}$  ions which belong to  $d^9$  states fills the orbitals either in  $e_g$  and  $t_{2g}$  states as per the Jahn–Teller distortion theory and helps in tuning the magnetic properties of ferrite nanopowders. The saturation magnetization ( $M_s$ ), coercivity ( $H_c$ ) and

retentivity ( $M_r$ ) determined from M-H curves. According to Neels' two sub-lattice model of ferrimagnetism, the A–B exchange interaction is dominant over A–A and B–B exchange interactions. The magnetic moment of metal ions at A and B sub-lattices are anti-parallel to each other and have a collinear spin arrangement. So the net magnetic moment per formula unit is calculated using the Eq. (2)

$$M_{\text{cal}} = M_B - M_A \quad (2)$$

Where  $M_{\text{cal}}$  is net calculated magnetic moment and  $M_A$  and  $M_B$  are the magnetic moment at the tetrahedral (A) and octahedral (B) sites. Magnetic moment values of  $\text{Fe}^{3+}$  ( $5 \mu\text{B}$ ) and  $\text{Cu}^{2+}$  ( $1 \mu\text{B}$ ) metal ions positioned at A and B lattice sites. The net magnetic moment for this comes out to be  $16 \mu\text{B}$ . One  $\text{Cu}^{2+}$  ion per unit cell on A site doubles the magnetic moment. But due to thermal quenching the magnetic moment increases beyond  $16 \mu\text{B}$  per unit cell. The observed magnetic moment ( $\eta_B$ ) has been calculated using the Eq. (3)

$$\eta_B = \frac{M_W \times M_S}{5585} \quad (3)$$

Where  $M_W$  is the molecular weight of the sample and  $M_S$  is saturation magnetization and the obtained value is 0.78. Magneto-crystalline anisotropy is intrinsic property of materials and it plays major role in coercivity. The anisotropy constant ( $K_\alpha$ ) was estimated according to Stoner–Wohlfarth theory [36] using the relation given below.

$$H_c = \frac{0.98 \times K_\alpha}{M_s} \quad (4)$$

The anisotropy constant estimated was  $3.27 \times 10^3 \text{ erg.cm}^{-3}$ . To know the isotropic nature of the sample, the remanence ratio of samples was estimated using  $R = M_R/M_R M_s \cdot M_s$  and found to be 0.222. Magnetic results confirm the partially inverted  $\text{CuFe}_2\text{O}_4$  particles with non-collinear spin structure and the decomposition of this ferrite into Fe–Cu–O phase leads to smaller quantity of CuO. Thus a low value of coercivity with moderate saturation magnetization can be achieved by using  $\text{Cu}^{2+}$  doped ferrite [37]. The use of  $\text{Cu}^{2+}$  ions for the preparation of ferrite should be beneficial not only for developing the simpler process but also tailoring its magnetic properties [38]. Our results can be further used for developing multi-functional nanocrystalline magnetites useful for effective adsorption.

## Adsorption studies

All adsorption studies were carried out using malachite green (MG) as the standard dye.

MG is basically a cationic dye which is classified as triarylmethane dye which exists in its chloride form. Its IUPAC name is 4-4-dimethylaminophenyl-phenyl

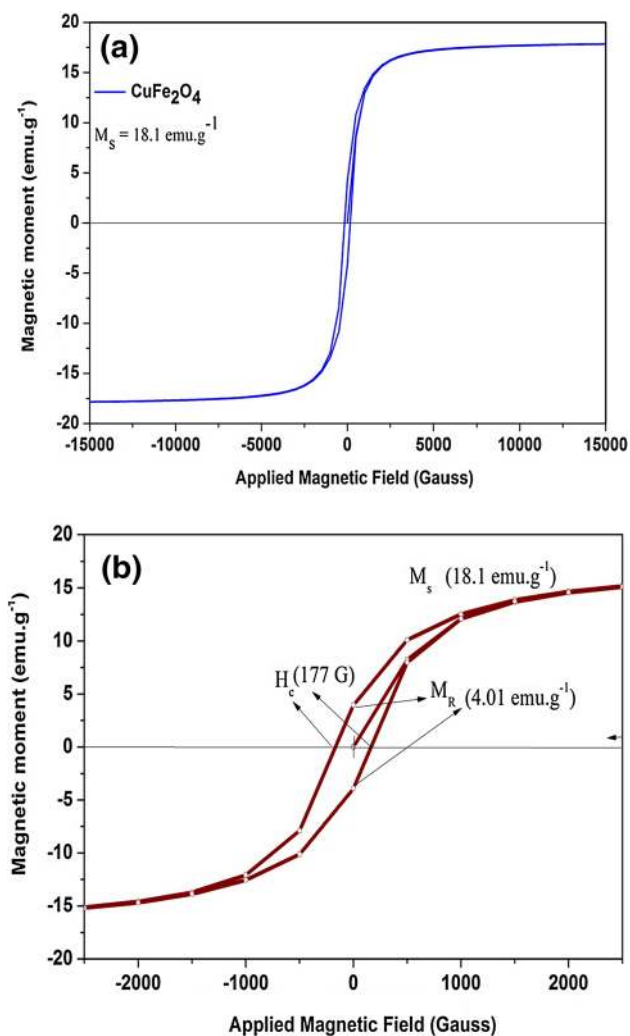


**Fig. 6** a M-H curves for  $\text{CuFe}_2\text{O}_4$ . b Enlarged M-H curve showing Coercivity, saturation magnetization



methylidene-1-cyclohexa-2,5-dienylidene-dimethylazanium chloride.  $\{C_6H_5 [CC_6H_4] (CH_3)_2\}Cl$  with a molecular weight of 327. The intense blue colour of the dye is due to its strong absorption in visible region at 618 nm.

Batch adsorption reactions were done in Borosil glass beakers covered with foil paper to avoid photolytic reaction and were stirred on a magnetic stirrer (250 rpm) at room temperature. The standard concentration of malachite green was taken as 10 ppm, from which different aliquots of the sample was taken of the experiment. The concentration of malachite green before and after each experiment was determined by measuring the absorbance in visible region using UV–Vis absorption spectrophotometer. Different parameters like dosage effect and stirring time were studied. All the adsorption studies were done in neutral pH.

Percentage of dye got adsorbed for different adsorbent loading is calculated using the Eq. (5).

$$\% \text{Adsorption} = \frac{(C_0 - C_e)}{C_e} \times 100 \quad (5)$$

where  $C_0$  is the initial dye concentration and  $C_e$  is the dye concentration after adsorption by copper ferrite nanoparticles after time  $t$  seconds.

The adsorption kinetics was studied by taking initial concentration of MG as 100 mL of 10 ppm which is allowed to react with combustion derived copper ferrite nanoparticles and stirred under dark for about 45 min. The equilibrium adsorption capacity  $q_e$  (mg/g) for a given weight of adsorbent (mg) is calculated according to the following Eq. (6)

$$q_e = (C_0 - C_e) \frac{V}{m} \quad (6)$$

Where  $C_0$  and  $C_e$  are the initial and equilibrium concentration of the dye respectively and  $V$  is the volume of dye solution and  $m$  is the mass of the adsorbent.

## Effect of nanoadsorbent loading

The optimum adsorbent concentration for the maximum and efficient adsorption of MG is done by varying the adsorbent weight and stirring under dark in similar conditions. 1000 mL of 10 ppm concentration of dye was prepared as stock solution. 100 mL of the stock solution is first stirred under dark without the adsorbent loading to see if any degradation takes place by itself and the absorbance of this solution is noted after 60 min which shows that no degradation of the dye. The effect of adsorbent loading is done by varying the amount of the nanoadsorbent from 5 to 50 mg and stirring it with 100 mL of dye solution under dark for 30 min. Time is kept constant for this batch study.

Figure 7a, b shows the influence of dosage of adsorbent loading on UV absorption and percentage adsorption of MG respectively, it is clear from both the graphs that as the amount of the adsorbent increases adsorption capacity also increases. However, batch adsorption studies shows that 85% MG adsorption was achieved for 40 mg of adsorbent loading. Further addition of the adsorbent is not showing much increase; still a slight increase in adsorption could be seen. This is attributed to the increase in the availability of more adsorption sites with increasing adsorbent dosage due to more available surface area, thereby leading to more binding sites for the adsorption of target pollutants onto the surface of the nanoadsorbent [39].

## Effect of contact time

To observe the time taken for the maximum adsorption of the dye on copper ferrite nanoadsorbent, we carried out the experiment at different time intervals by keeping constant weight of 30 mg copper ferrite nanoparticle and the experiment was carried out by varying time of contact. Small aliquot of the reaction mixture was removed every

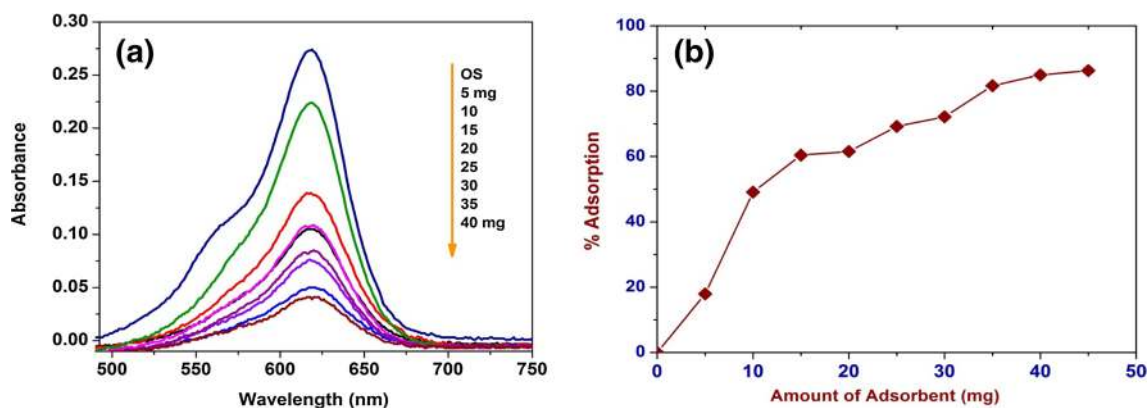


**Fig. 7** a Dosage effect graph (dosage of  $CuFe_2O_4$  from 5 to 40 mg). b Percentage adsorption of MG dye at different adsorbent ( $CuFe_2O_4$ ) loading



5 min and centrifuged at 20,000 rpm for 10 min to remove the adsorbent particles and measured the absorbance by UV–Vis spectrophotometer. It is observed that the absorption of light decreased with time and rapid adsorption had taken place in 15 min and reached equilibrium by 30 min. The equilibrium data collected shows that the percentage of adsorption increased with respect to time which is shown in the Fig. 8.

### pH at point zero charge (pH PZC) and mechanism of adsorption

The  $\text{pH}_{\text{PZC}}$  results of the experiments performed with the  $\text{CuFe}_2\text{O}_4$  adsorbent, where the pH ranged from 2 to 9. The  $\text{pH}_{\text{PZC}}$  of the  $\text{CuFe}_2\text{O}_4$  is found to be 5.4 (figure not

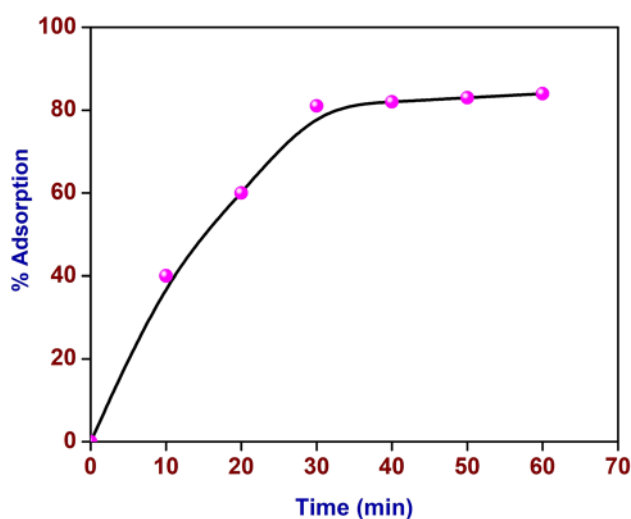
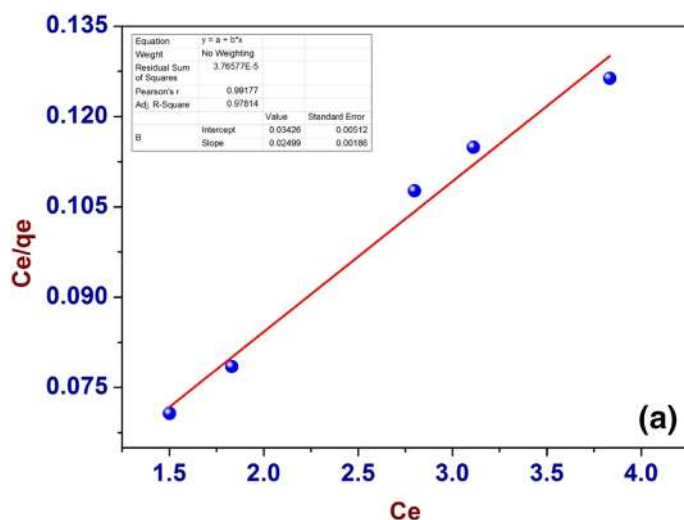


Fig. 8 Percentage adsorption of MG dye at different contact time



shown), which indicates that below the  $\text{pH}_{\text{PZC}}$  value, the surface of  $\text{CuFe}_2\text{O}_4$  is positively charged due to protonation [40], favoring the adsorption of anions. Above the  $\text{pH}_{\text{PZC}}$ , the  $\text{CuFe}_2\text{O}_4$  surface has a negative charge which favors the adsorption of cation species. In present case we have carried out the batch adsorption experiments at neutral pH and the MG is a cationic dye. Since the  $\text{pH}_{\text{PZC}}$  is 5.4 above which the surface of  $\text{CuFe}_2\text{O}_4$  is positively charged hence favors the adsorption of cationic species MG.

### Adsorption modeling

Adsorption isotherm is the study of the relation between the amounts of adsorbate, adsorbed on the surface of adsorbent and temperature. Adsorption isotherm was studied by Langmuir-Hinshelwood model to know the rate constant of adsorption of MG on combustion derived CF nanoparticles. In the present study Langmuir [41] and Freundlich [42] adsorption isotherm models are used to investigate the adsorption of MG on combustion derived CF nanoadsorbent. Figure 9a, b gives the Langmuir and Freundlich adsorption isotherm graphs. The results are well in accordance with Langmuir model ( $R^2 = 0.978$ ) than the Freundlich model ( $R^2 = 0.831$ ) values obtained. Therefore, we have elaborated the discussion on the Langmuir model.

### Langmuir isotherm

This model gives an insight into the specific number of sites where the adsorption can take place and to quantify the amount of adsorbate adsorbed on the nanoadsorbent at a given

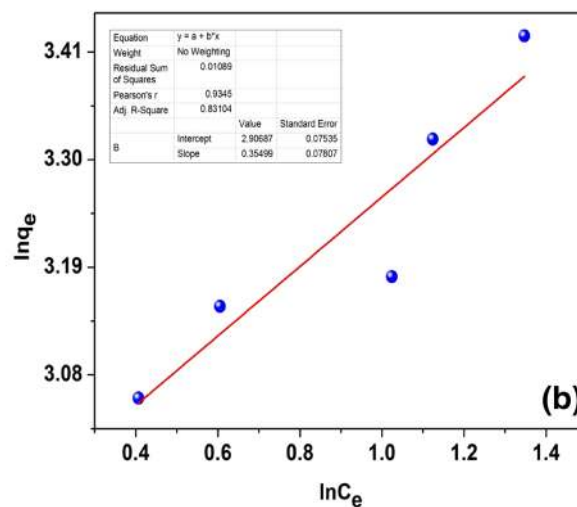
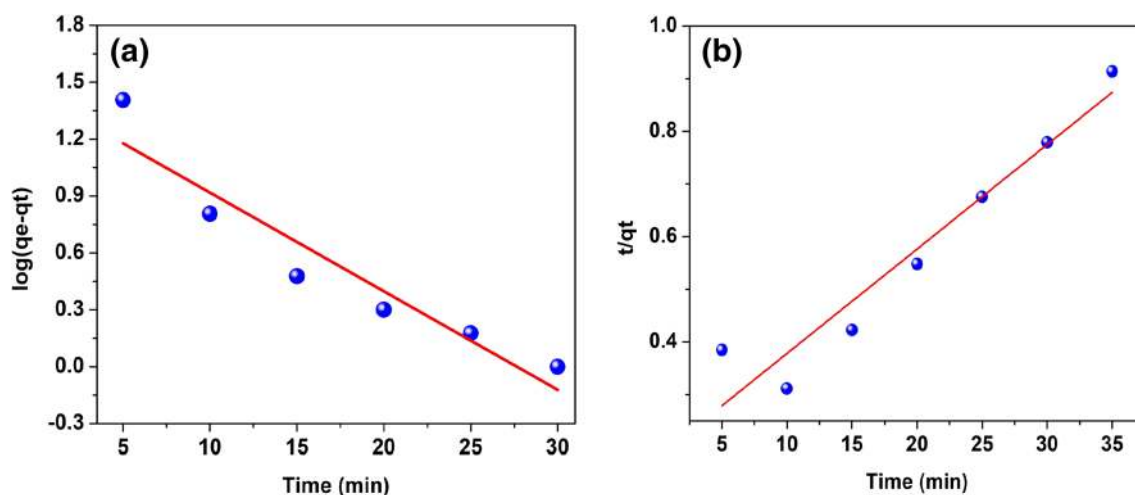


Fig. 9 a Langmuir, b Freundlich adsorption isotherms





**Fig. 10** **a** Pseudo first order. **b** Pseudo second order kinetics plot for the adsorption of MG on to the copper ferrite

temperature. Also it helps to find whether the adsorption is of monolayer or multilayer adsorption. The Langmuir equation is given in the following equation.

$$\frac{C_e}{Q_e} = \frac{1}{Q_0 b} + \frac{C_e}{Q_0} \quad (7)$$

Where  $C_e$  is the equilibrium concentration (mg/L),  $Q_e$  is the amount of dye adsorbed at equilibrium,  $Q_0$  is the monolayer adsorption capacity and  $b$  is the energy of adsorption constant called as Langmuir constant. Figure 9a gives Langmuir plot of  $C_e/Q_e$  versus  $C_e$  which is a linear graph.  $R^2$  value = 0.978 obtained from the graph confirms the applicability of Langmuir isotherm thus concluded that it involves monolayer adsorption with no lateral interaction between the adsorbed molecules.

The Langmuir constants  $Q_0$  and  $b$  were determined from the slope and intercept of the plot and value shows the maximum adsorption capacity produced from the saturated monolayer coverage of adsorbate molecule on the adsorbent surface.

To confirm the favorability of the adsorption process another parameter called equilibrium parameter  $R_L$  also called separation factor, was calculated from Langmuir's equation as follows.

$$R_L = \frac{1}{1 + bC_0} \quad (8)$$

where  $C_0$  is the adsorbate concentration. The  $R_L$  value obtained from the graph will help us to conclude the favorability of adsorptions. For favorable adsorption  $R_L$  should be between 0–1 and  $> 1$  shows unfavorable adsorption. We obtain the slope =  $1/Q_0 = 0.00829$  and the intercept =  $1/Q_0 b = 0.0085$ . Therefore  $Q_0 = 120.62$  and the  $b = 0.9749$  and the  $R_L = 1/1 + bC_0 = 0.09$ . The present

studies shows that  $R_L = 0.09$  which is very much in agreement with the favorable conditions for adsorption. The adsorption capacity for the  $\text{CuFe}_2\text{O}_4$  is found to be 22 mg/g [43].

### Adsorption kinetics

Kinetics of adsorption is an important characteristic in explaining the efficiency of sorption. It explains solute uptake rate, which in turn governs the residence time of the reaction [44]. In order to understand the reaction mechanism of adsorption of malachite green on copper ferrite nanopowder is studied by both 1st order (Fig. 10a) and pseudo 2nd order kinetics (Fig. 10b) are studied and is explained as follows. For 1st order kinetics,

$$r = \frac{-dc}{dt} = \frac{k_r KC}{(1 + KC)r} \quad (9)$$

where  $r$  is the rate of adsorption,  $k_r$  is the adsorption coefficient of the reactant,  $K$  is adsorption coefficient of the reactant and  $C$  is the reactant concentration. But when  $C$  is very small, the above equation can be expressed as

$$r = \frac{-dc}{dt} = k_r KC = kC \quad (10)$$

where  $k$  is the first order rate constant. When  $t = 0$ ,  $C = C_0$ , therefore the above Eq. (10) becomes

$$\frac{\ln C_0}{C} = kt \quad (11)$$



Figure 10a shows that the first order kinetics is not fitting for this sorption process. Therefore the adsorption kinetics is explained by pseudo second order mechanism.

### Pseudo second order

The adsorption kinetics of MG on CF nanoparticles is best explained by pseudo second order rate kinetics which is fitting with the results we got. This suggests that the adsorption rate is affected by the concentration of both dye concentration and the adsorption sites on the adsorbent [45], which is expressed as follows

$$\frac{t}{q_t} = \frac{1}{k_2 q_e^2} + \frac{1}{q_e} \cdot t \quad (12)$$

where  $q_e$  and  $q_t$  are the amount of MG adsorbed at equilibrium and at time  $t$  respectively,  $k_2$  is the rate constant of the pseudo second order kinetics model of adsorption (g/mg/min). The adsorption kinetics graph is given in Fig. 10 which gives a linear plot that suggests the pseudo second order model. Slope is calculated from the graph as  $1/q_e = 0.01983$ . Therefore  $q_e = 50.42$ . This accounts that the adsorption is rapid in the first 15 min and further the rate of adsorption is relatively slower and after 30 min it attains equilibrium. The initial high rate of adsorption is attributed to the high porosity and surface area of combustion derived CF nanoparticles.

### Recyclability and stability of the adsorbent

An adsorbent is considered as efficient and economical if it shows considerable retention of adsorption capacity. For the application of adsorbent for the real time samples it is expected the adsorbent should retain its adsorption capacity after multiple runs. The recyclability and stability  $\text{CuFe}_2\text{O}_4$  adsorbent for the removal of MG is carried out and the results are presented in Fig. 11. The  $\text{CuFe}_2\text{O}_4$  adsorbent after the batch adsorption was filtered using ashless filter paper, washed with deionised water and then heated in order to eliminate the adsorbed MG dye molecules and restore adsorbent surface. Figure 11a shows the results obtained for recycling experiments and from the graph it is evident that up to three cycles there is minimum loss in the removal of MG. However, after three cycles there is considerable decrease in the removal efficiency of MG. The observed decrease might be due to the loss of adsorption sites during regeneration process. The stability of adsorbent after recycling was carried out using FT-IR and the results are shown in Fig. 11b. From the FT-IR spectra it is evident that the adsorbent shows well defined bands at 528 and 451  $\text{cm}^{-1}$

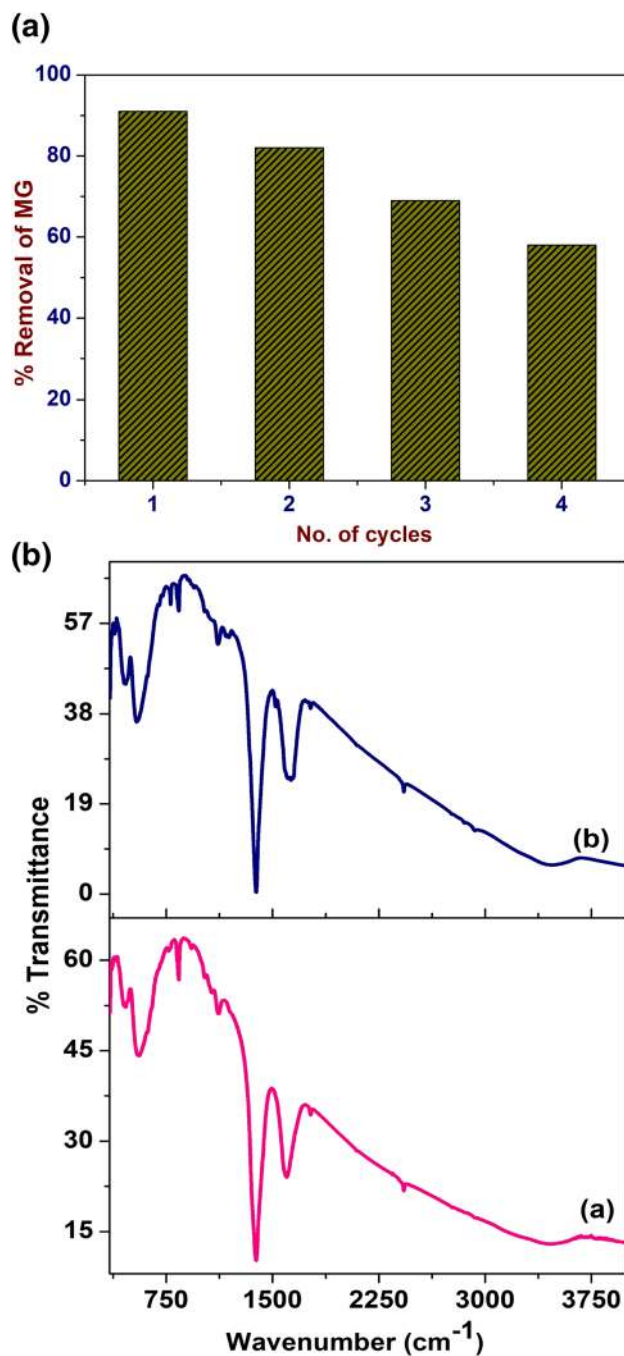


**Fig. 11** A Percentage removal of MG for regenerated adsorbent at different cycle runs. B FT-IR spectra of regenerated  $\text{CuFe}_2\text{O}_4$  (a) 1st cycle, (b) 3rd cycle

corresponding to octahedral group Fe–O and tetrahedral group Cu–O stretching respectively. These bands are similar to the bands obtained for pure  $\text{CuFe}_2\text{O}_4$  (Fig. 2). These

results confirm that even after the recycling the  $\text{CuFe}_2\text{O}_4$  is stable.

## Conclusion

A novel nano adsorbent  $\text{CuFe}_2\text{O}_4$  was synthesised by solution combustion synthesis and used for adsorption of malachite green cationic dye. Structural and morphological characterizations revealed spinal cubic structure and porous morphology of  $\text{CuFe}_2\text{O}_4$  adsorbent. Batch adsorption studies showed that adsorption of MG depends on various physio-chemical parameters such as adsorbent loading, contact time. Adsorption kinetics results show that adsorption of MG over copper ferrite follows pseudo second order kinetics. Using the Langmuir isotherm a maximum adsorption capacity of 200 mg/g is calculated. 40 mg of CF is sufficient for 85% removal of MG dye in 30 min at neutral pH. Further, the magnetic studies of the copper ferrite studied by M-H curves shows the magnetic nature of adsorbent. Thus it can be used as magnetically recoverable nanoadsorbent for the removal of malachite green by adsorption technique from effluent water.

**Open Access** This article is distributed under the terms of the Creative Commons Attribution 4.0 International License (<http://creativecommons.org/licenses/by/4.0/>), which permits unrestricted use, distribution, and reproduction in any medium, provided you give appropriate credit to the original author(s) and the source, provide a link to the Creative Commons license, and indicate if changes were made.

## References

- Rajeshkannan, R.: Decolourization of malachite green—optimization, isotherm and kinetic studies. *Chem. Ind. Chem. Eng.* **17**, 67–79 (2011)
- Ali, I., Al-Othman, Z.A., Alwarthan, A.: Molecular uptake of congo red dye from water on iron composite nano particles. *J. Mol. Liq.* **224**, 171–176 (2016)
- Khan, T.A., Sharma, S., Ali, I.: Adsorption of rhodamine B dye from aqueous solution onto acid activated mango (*Mangifera indica*) leaf powder: equilibrium, kinetic and thermodynamic studies. *J. Toxicol. Environ. Health* **3**(10), 286–297 (2011)
- Ali, I., Gupta, V.K.: Advances in water treatment by adsorption technology. *Nat. Protoc.* **1**, 2661–2667 (2006)
- Culp, S.J.: Mutagenicity and carcinogenicity in relation to DNA adduct formation in rats fed leucomalachite green. *Mutat. Res.* **506–507**, 55–63 (2002)
- Srivastava, S.: Toxicological effects of malachite green. *Aquat. Toxicol.* **66**(3), 319–329 (2004)
- Ali, I., Al-Othman, Z.A., Alwarthan, A.: Green synthesis of functionalized iron nano particles and molecular liquid phase adsorption of ametryn from water. *J. Mol. Liq.* **221**, 1168–1174 (2016)
- Ali, I., Al-Othman, Z.A., Alwarthan, A.: Synthesis of composite iron nano adsorbent and removal of ibuprofen drug residue from water. *J. Mol. Liq.* **219**, 858–864 (2016)
- Ali, I., AlOthman, Z.A., Sanagi, M.M.: Green synthesis of iron nano-impregnated adsorbent for fast removal of fluoride from water. *J. Mol. Liq.* **211**, 457–465 (2015)
- Ali, I., Al-Othman, Z.A., Alwarthan, A.: Supra molecular mechanism of the removal of 17- $\beta$ -estradiol endocrine disturbing pollutant from water on functionalized iron nano particles. *J. Mol. Liq.* **441**, 123–129 (2017)
- Chandran, D.: A review of the textile industries waste water treatment methodologies. *Int. J. Sci. Eng. Res.* **7**(1), 2229–5518 (2016)
- Ali, I.: New generation adsorbents for water treatment. *Chem. Rev.* **112**, 5073–5091 (2012)
- Ali, I., Asim, M., Khan, T.A.: Removal of chromium(VI) from aqueous solution using guar gum–nano zinc oxide biocomposite adsorbent. *Arabian J. Chem.* **10**, 2388–2398 (2017)
- Ali, I.: Water treatment by adsorption columns: evaluation at ground level. *Sep. Purif. Rev.* **43**, 175–205 (2014)
- Khan, T.A., Nazir, M., Ali, I., Kumar, A.: Removal of chromium(VI) from aqueous solution using guar gum–nano zinc oxide biocomposite adsorbent. *Arabian J. Chem.* (2013)
- Sugimogo, M.: Past, present & future of ferrites. *J. Am. Ceram. Soc.* **82**, 269–280 (1999)
- Raj, K.: Advances in ferrofluid technology. *J. Magn. Magn. Mater.* **149**, 174–180 (1995)
- Singh, A.: Synthesis, characterization, magnetic properties and gas sensing applications of  $\text{Zn}_x\text{Cu}_{1-x}\text{Fe}_2\text{O}_4$  nanocomposites. *Mater. Sci. Semicond. Process.* **27**, 934–949 (2014)
- Kharisov, B.I.: Solubilization, dispersion and stabilization of magnetic nanoparticles in water and non-aqueous solvents: recent trends. *RSC Adv* **4**, 45354–45381 (2014)
- Prashanth, P.A., Raveendra, R.S.: Synthesis, characterizations, antibacterial and photoluminescence studies of solution combustion-derived  $\alpha\text{-Al}_2\text{O}_3$  nanoceramic. *J. Asian Ceram. Soc.* **3**, 345–351 (2015)
- Monika, D.L., Nagabhushana, H., Sharma, S.C., Nagabhushana, B.M., Hari Krishna, R.: Synthesis of multicolor emitting  $\text{Sr}_{2-x}\text{Sm}_x\text{CeO}_4$  nanophosphor with compositionally tuneable photo and thermoluminescence. *Chem. Eng. J.* **253**, 155–164 (2014)
- Patil, K.C.: Combustion synthesis—an update. *Solid State Mater. Sci.* **6**, 507–512 (2002)
- Puangpetch, T., Sreethawong, T., Yoshikawa, S., Chavadej, S.: Synthesis and photocatalytic activity in methyl orange degradation of mesoporous-assembled  $\text{SrTiO}_3$  nanocrystals prepared by sol-gel method with the aid of structure-directing surfactant. *J. Mol. Catal. A Chem.* **287**, 70–79 (2008)
- Greene, D.: Synthesis and characterization of  $\text{CoFe}_2\text{O}_4\text{-SiO}_2\text{-TiO}_2$  nanocomposites. *Nanomaterials* **4**, 331–343 (2014)
- Viswanath, I.V.K.: Synthesis and characterization of nanoferrites. *Int. J. Chem. Sci.* **11**(1), 64–72 (2013)
- Lopez-Ramon, M.V., Stoeckli, F., Moreno-Castilla, C., Carrasco-Marin, F.: On the characterization of acidic and basic surface sites on carbons by various techniques. *Carbon* **37**, 1215–1221 (1999)
- Yao-Jen, T.: Strontium removal in seawater by means of composite magnetic nanoparticles derived from industrial sludge. *Water* **8**, 357 (2016)
- Aziz, H.S.: Evaluation of electrical, dielectric and magnetic characteristics of Al–La doped nickel spinel ferrites. *RSC Adv.* **6**, 6589–6597 (2016)
- Verwey, E.J.W.: Physical properties and cation arrangement of oxides with spinel structures. *J. Chem. Phys.* **15**, 174 (1947)
- Klug, H.P.: X-ray diffraction procedures: for polycrystalline and amorphous materials, 2nd edn. Wiley, New York (1974). ISBN 978-0-471-49369-3
- Saikia, B.J.: Fourier transform infrared spectroscopic characterization of kaolinite. *J. Mod. Phys.* **1**, 206–210 (2010)



32. Tehrani, F.S.: Structural, magnetic, and optical properties of zinc- and copper-substituted nickel ferrite nanocrystals. *J. Supercond. Novel Magn.* **25**, 2443–2455 (2012)
33. Zhang, X.: Infrared absorption spectra of the CO<sub>2</sub>/H<sub>2</sub>O complex in a cryogenic nitrogen matrix-detection of a new bending frequency. *J. Phys. Chem. A* **115**, 9854–9860 (2011)
34. Hari Krishna, R., Nagabhushana, B.M., Nagabhushana, H., Chakradhar, R.P.S., Sivaramakrishna, R., Shivakumara, C., Thomas, T.: Auto-ignition based synthesis of Y<sub>2</sub>O<sub>3</sub> for photo- and thermo-luminescent applications. *J. Alloys Compd.* **585**, 129–137 (2014)
35. Ghosh, S.K.: Effect of fuel characteristics on synthesis of calcium hydroxyapatite by solution combustion route. *Bull. Mater. Sci.* **33**(1), 7–16 (2010)
36. Haralkar, S.J.: Substitutional effect of Cr<sup>3+</sup> ions on the properties of Mg–Zn ferrite nanoparticles. *Phys. B Condens. Matter* **407**, 4338–4346 (2012)
37. Kanakaraj, M.: Structural and magnetic properties of CuFe<sub>2</sub>O<sub>4</sub> as-prepared and thermally treated spinel nanoferrites. *Indian J. Pure Appl. Phys.* **52**, 124–130 (2014)
38. Lakhani, V.K.: Structural parameters and X ray Debye temperature determination study on copper–ferrite–aluminates. *Solid State Sci.* **13**, 539–547 (2011)
39. Hassani, A., Khataee, A., Karaca, S., Karaca, M., Kiranşan, M.: Adsorption of two cationic textile dyes from water with modified nanoclay: a comparative study by using central composite design. *J. Environ. Chem. Eng.* **3**, 2738–2749 (2015)
40. Ng, H.W., Lee, L.Y., Chan, W.L., Gan, S., Chemmangattuvallappil, N.: *Luffa acutangula* peel as an effective natural biosorbent for malachite green removal in aqueous media: equilibrium, kinetic and thermodynamic investigations. *Desalination Water Treat.* **57**, 7302–7311 (2016)
41. Langmuir, I.: The adsorption of gases on plan surfaces of glass, mica and platinum. *J. Am. Chem. Soc.* **40**, 1361–1403 (1918)
42. Freundlich, H.M.F.: Over the adsorption in solution. *J. Phys. Chem.* **57**, 85–470 (1906)
43. Senthilkumaar, S., Varadarajan, P.R.: Adsorption of methylene blue onto jute fiber carbon: kinetics and equilibrium studies. *J. Colloid Interface Sci.* **284**, 78–82 (2005)
44. Hema, M.: Adsorption kinetics and thermodynamics of malachite green onto acid activated low cost carbon. *J. Appl. Sci. Environ. Manag.* **12**, 43–51 (2008)
45. Wang, T.: Cu doped Fe<sub>3</sub>O<sub>4</sub> magnetic adsorbent for arsenic: synthesis, property, and sorption application. *RSC Adv.* **62**, 50011–50018 (2015)

**Publisher's Note** Springer Nature remains neutral with regard to jurisdictional claims in published maps and institutional affiliations.

## Affiliations

Bincy Rose Vergis<sup>1,2</sup> · R. Hari Krishna<sup>1</sup> · Nagaraju Kottam<sup>1</sup> · B. M. Nagabhushana<sup>1</sup> · R. Sharath<sup>3</sup> · B. Darukaprasad<sup>4</sup>

✉ R. Hari Krishna  
rhk.chem@gmail.com

✉ Nagaraju Kottam  
knrmsr@gmail.com

<sup>1</sup> Department of Chemistry, M.S. Ramaiah Institute of Technology (Autonomous Institute affiliated to Visvesvaraya Technological University, Belagavi-590 014), Bangalore 560 054, India

<sup>2</sup> Department of Chemistry, B.M.S. Institute of Technology and Management, Bangalore 560 064, India

<sup>3</sup> Department of Biotechnology, M.S. Ramaiah Institute of Technology, Bangalore 560 054, India

<sup>4</sup> Department of Physics, B. M. S. Institute of Technology and Management, Bangalore 560 064, India

